Atomic-scale study of the adsorption of calcium fluoride on Si(100) at low-coverage regime

Franco Chiaravalloti,[1] Gérald Dujardin,[1] Damien Riedel,[1,*] Henry P. Pinto,[2] and Adam S. Foster[3,4]

[1]*Institut des Sciences Moléculaires d'Orsay, UMR 8214, Université Paris Sud, 91405 Orsay Cedex, France*

[2]*Interdisciplinary Center for Nanotoxicity, Department of Chemistry, Jackson State University, Jackson, Mississippi 39217-0510, USA*

[3]*Department of Applied Physics, Aalto Scool of Science, P.O. Box 11100, FI-00076 Aalto, Finland*

[4]*Department of Physics, Tampere University of Technology, P.O. Box 692, FI-33010 Tampere, Finland*

(Received 15 June 2011; revised manuscript received 12 September 2011; published 18 October 2011)

We investigate, experimentally and theoretically, the initial stage of the formation of Ca/Si and Si/F structures that occurs during the adsorption of CaF_2 molecules onto a bare Si(100) surface heated to 1000 K in a low-coverage regime (0.3 monolayer). A low-temperature (5 K) scanning tunneling microscope (STM) is used to observe the topographies and the electronic properties of the exposed silicon surfaces. Our atomic-scale study reveals that several chemical reactions arise during CaF_2 deposition, such as dissociation of the CaF_2 molecules and etching of the surface silicon dimers. The experimental and calculated STM topographies are compared using the density functional theory, and this comparison enables us to identify two types of reacted structures on the Si(100) surface. The first type of observed complex surface structure consists of large islands formed with a semiperiodic sequence of 3×2 unit cells. The second one is made of isolated Ca adatoms adsorbed at specific sites on the Si(100)-2×1 surface.

DOI: 10.1103/PhysRevB.84.155433 PACS number(s): 81.15.Hi, 73.61.Wp, 31.70.Ks, 68.37.Ef

I. INTRODUCTION

Controlling the thickness, morphology, homogeneity, and purity of epitaxial ultrathin layers on semiconductors is of crucial importance in many domains, including nanoelectronics,[1] light-emitter architectures,[2] and in the fabrication of nanophotonic structures.[3] In particular, the use of thin insulating layers of CaF_2 on Si(111) in the design of three-dimensional electronic devices[4] has led to many experimental[5] and theoretical[6] investigations into its growth in the past 20 years. More recently, the study of the formation of CaF_2 structures on Si(100) surfaces has come to prominence.[7–11] While for the Si(111) surface, the formation of isotropic CaF_2 islands is readily achieved, the Si(100) surface offers the possibility for growth of long fluorite stripes with good electronic insulating properties.[11] In both cases, investigations of these substrates have shown the crucial importance of a deep understanding of the growth processes in order to achieve their control and develop new applications at the nanoscale.[12] However, whereas the formation of the CaF_2/Si(111) interface is well documented, the initial stage of the wetting layer formation on Si(100) is still poorly understood at the nanoscale. This is particularly true for low-coverage rates and for substrate temperature above 900 K, i.e., outside the Volmer-Weber regime.

In this paper, we focus our investigations on the initial stage of the formation of the wetting layer at low coverage (0.3 monolayer [ML]) and other related products when a bare Si(100) surface heated at 1000 K is exposed to CaF_2 molecules. For this purpose, we use a low-temperature (5 K) scanning tunneling microscope (STM) to investigate the atomic structure of the first step of Stransky-Krastanov island growth. Our experiments reveal two main types of surface structures. One of them is built with a repeated unit cell semiperiodically arranged on the surface consisting of one missing silicon dimer replaced by a single Ca atom together with a silicon dimer having two Si-F bonds. The second structure consists of single Ca adatoms regularly localized on top of the silicon surface. Our theoretical investigations performed using the density functional theory (DFT) along with calculation of STM topographies confirm our experimental observations and allow clarification of the observed surface structures at the atomic scale.

II. EXPERIMENTAL AND THEORETICAL METHODS

For these experiments, we use n-doped (As, $\rho = 0.004\ \Omega{\cdot}$cm) silicon samples prepared in ultrahigh vacuum (2.0×10^{-11} torr). Following the cleaning and the reconstruction processes of the bare Si(100) surface,[13] the sample is transferred into the STM to check its 2×1 reconstruction and especially the presence of a relatively low number of defects.[14] The CaF_2 molecules used for these experiments are evaporated from small fluorite crystals (Goodfellow) using a graphite effusion cell (MBE-Komponenten) heated to ~1330 K. Throughout the evaporation process, the crucible holder is cooled by an external water flow to optimize the control of its temperature. The flux of the CaF_2 molecular beam is calibrated before each evaporation with a quartz microbalance. This calibration leads to a covering rate of ~1 Å min^{-1}. Following the calibration, the bare silicon surface is extracted from the STM and placed at ~10 cm from the effusion cell, in replacement of the quartz balance. With this procedure, we can precisely direct the molecular beam onto the silicon surface. Then, the silicon surface is set at a constant temperature of ~1000 K by resistive heating. Following these preparations, the silicon surface is exposed to the CaF_2 molecular beam for 15 seconds at a base pressure of $\sim 7 \times 10^{-11}$ torr, which corresponds to a surface coverage of ~0.3 ML.[11] The silicon sample is then cooled down to 12 K and transferred into the STM to be analyzed. Our results are the repeated analysis of five different samples and STM tips.

The theoretical calculations are performed using the plane-wave basis Vienna ab-initio simulation package (VASP)[15,16] implementing DFT and the generalized gradient approximation (GGA) by Perdew, Burke, and Ernzerhof (PBE).[17] We describe the Si-[Ne], F-$1s^2$, and Ca-[Ne] $3s^2$ core electrons

with projector-augmented wave (PAW) potentials.[18] Using a cutoff kinetic energy of 400 eV and a Monkhorst–Pack k-point mesh with a separation of 0.02 $Å^{-1}$, we converge the total energy to values below 1 meV/f.u. (f.u. = formula unit Si-fcc). The ionic optimizations are performed until all the forces on relaxed atoms are below 0.01 eV $Å^{-1}$.

We first optimize the bulk Si-fcc structure with a predicted lattice constant of 5.43 Å.[19] From this structure, we build the Si(100) surface using periodic slabs, five layers thick, separated by 15 Å along the (100) axis. The Si atoms at the bottom layer are passivated with hydrogen, and this Si-H layer is kept frozen during all the relaxations. We model the Ca adatoms on the Si(100) surface with a 5×4 Si(100) slab, while the Ca-F/Si(100) interface is more accurately described with a 3×2 Si(100) slab. The second step of our theoretical work consists of computing constant-current mode STM images and the line scans for the aforementioned slabs. For this purpose, we use the Tersoff-Hamann approximation[20] as implemented in the bSKAN code.[21] It employs the real-space single-electron wave functions of the slabs computed previously with VASP.

III. RESULTS AND DISCUSSIONS

As explained in the previous section, the bare surface of the Si(100) 2×1 is initially observed with the STM to check the presence of a low rate of surface defects[14] (usually less than 1%, Fig. 1(a)) prior to each CaF_2 evaporation. After the CaF_2

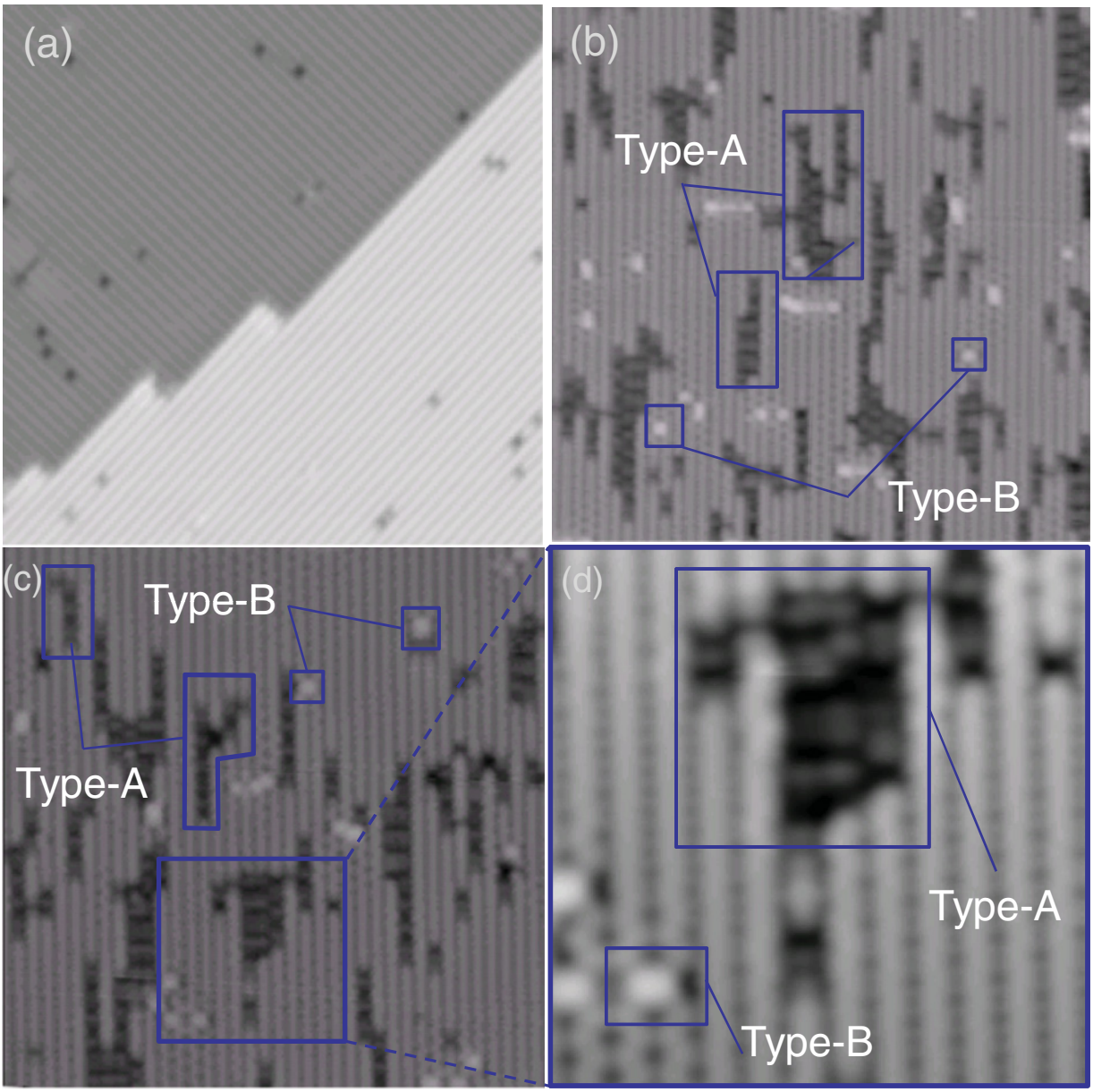

FIG. 1. (Color online) (a) 260 × 260 $Å^2$ ($V_s = -1.5$ V, I = 61 pA) STM topography of the bare Si(100) at 5 K. (b) 340 × 340 $Å^2$, (c), 290 × 290 $Å^2$, and (d) and 93 × 93 $Å^2$ ($V_s = -2.0$ V, I = 76 pA) STM topographies of the Si(100) surface at 5 K after a deposition of 0.3 monolayer of CaF_2 molecules, respectively. The structures of type-A and the bright protrusions of type-B are indicated.

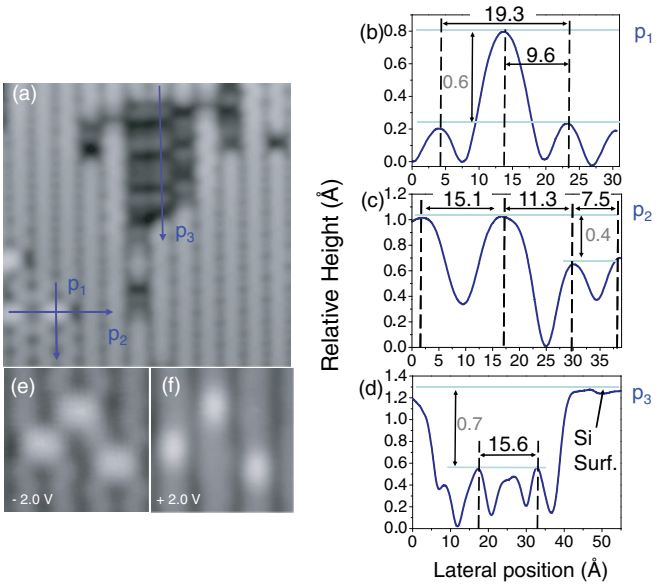

FIG. 2. (Color online) (a) 93 × 93 Å^2 STM topography (V_s = −2.0 V, I = 76 pA) of the exposed Si(100) surface showing three line scans along p_1, p_2, and p_3. (b), (c), and (d) Relative averaged height measured along the profiles p_1, p_2, and p_3, respectively. (e) and (f) 35 × 35 Å^2 occupied (V_s = −2.0 V, I = 100 pA) and unoccupied (V_s = +2.0 V, I = 100 pA) state STM topographies of the structures of type-B.

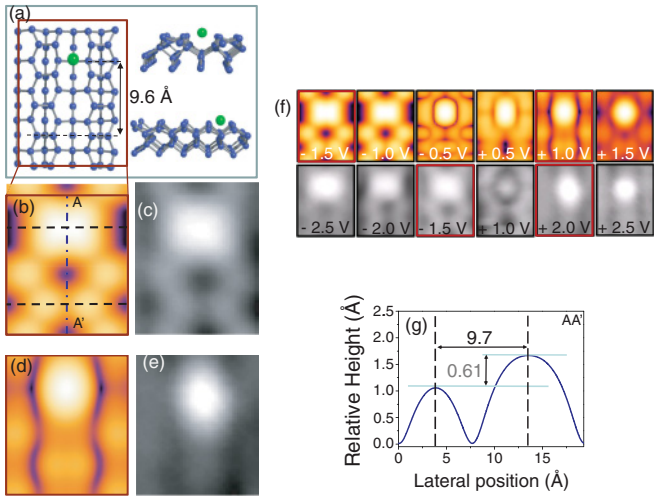

FIG. 3. (Color online) (a) Top and side views of the 4 × 5 silicon supercell in ball-and-stick model used to calculate the Ca adatom structure. The blue balls are silicon atoms, and the green ball is a Ca atom. (b) and (c) 10 × 17 Å^2 calculated (V_{theo} = −1.5 V) and experimental (V_s = −1.5 V) occupied state STM topographies of the supercell defined in (a). (d) and (e) 10 × 17 Å^2 calculated (V_{theo} = +1.0 V) and experimental (V_s = +2.0 V) unoccupied state STM topographies of the corresponding supercell defined in (a). (f) Comparison between observed and computed STM images for a series of bias voltages V_s = −2.5, −2.0, −1.5, +1.0, +2.0, and +2.5 V, and V_{theo} = −1.5, −1.0, −0.5, +0.5, +1.0, and +1.5 V. (g) Calculated profile along the A-A′ section defined in (b).

exposure, the occupied state STM topographies (Fig. 1(b)) show two types of new features. As observed in Figs. 1(b) and 1(c), the silicon surface is covered with dark areas (type-A), which are structured like a discontinuous arrangement of small unit cells. They are formed in alignment with respect to the silicon dimer row orientation. Smaller bright features (type-B) are also observed on the silicon surface and are located beside the features of type-A [Figs. 1(b) and 1(c)]. A closer look at these structures allows the observation of their internal arrangement in more detail (Figs. 1(c) and 1(d)). For example, the dark areas of type-A appear to be fabricated with elements arranged quasiperiodically, while a single element of the bright features of type-B appears to be precisely located in between the silicon dimer rows (Figs. 1(d)). Note the buckling of the neighbor silicon dimers observed nearby the single bright features of type-B (Fig. 1(d)), which usually indicates a weak bonding between an adsorbate and the Si(100) surface.[22,23]

Figure 2 presents a deeper analysis of both structures via the measure of various relative height profiles. The relative averaged heights measured along p_1 to p_3 are reported in Figs. 2(b) to 2(d) and are representative of observations from all the tested samples. The profile p_1 in Fig. 2(b) measured along the silicon back-bonds row and crossing the features of type-B reveals a protrusion on the buckled silicon surface with a relative height of ∼0.6 Å (V_s = −2 V). The measure of the relative distance between the two buckled silicon dimers that are adjacent to the bright feature of type-B is 19.3 Å, and this represents the distance separating five consecutive silicon dimers, i.e., 3.85 Å × 5. From Fig. 2(b), we can observe that the feature of type-B is located at the middle of this distance (9.6 Å), i.e., 2.5 × 3.85 Å.[14] This indicates that the bright feature is positioned in the silicon back-bonds and in between two silicon dimers. This is confirmed by a comparison of the STM topographies in the occupied and unoccupied states (Figs. 2(e) and 2(f)). The profile p_2 in Fig. 2(c), measured on the same protrusion across the dimer rows, reveals that the distance between the two observed bright features is ∼15 Å, which is consistent with the distance separating two silicon back-bonds rows. However, the profile p_3, measured along a silicon dimer row surrounding a feature of type-A, reveals an apparent height of this structure located 0.7 Å below the silicon surface, which is materialized here by the unbuckled silicon dimer row.

We now concentrate on the structure of type-B. As will be discussed later in the paper, and as previously reported,[11] one can anticipate that several Ca atoms resulting from the dissociation of CaF_2 molecules will be adsorbed onto the silicon surface. Considering the previous experimental observations, our theoretical investigation allows us to test a configuration that corresponds to a single Ca adatom located in between the silicon dimer rows and between two silicon dimers as described in Fig. 3(a). The ensuing calculated STM topographies (Figs. 3(b) and 3(d)) can be compared with the experimental STM topographies of the features of type-B observed on the Si surface with a very reasonable agreement (Figs. 3(c) and 3(e)). Indeed, our calculations reproduce clearly both the occupied state (Figs. 3(b) and 3(c)) and the unoccupied state (Figs. 3(d) and 3(e)) STM topographies. A series of calculated STM images can be compared with experimental topographies at various surface voltages (Fig. 3(f)). The slight differences observed in the

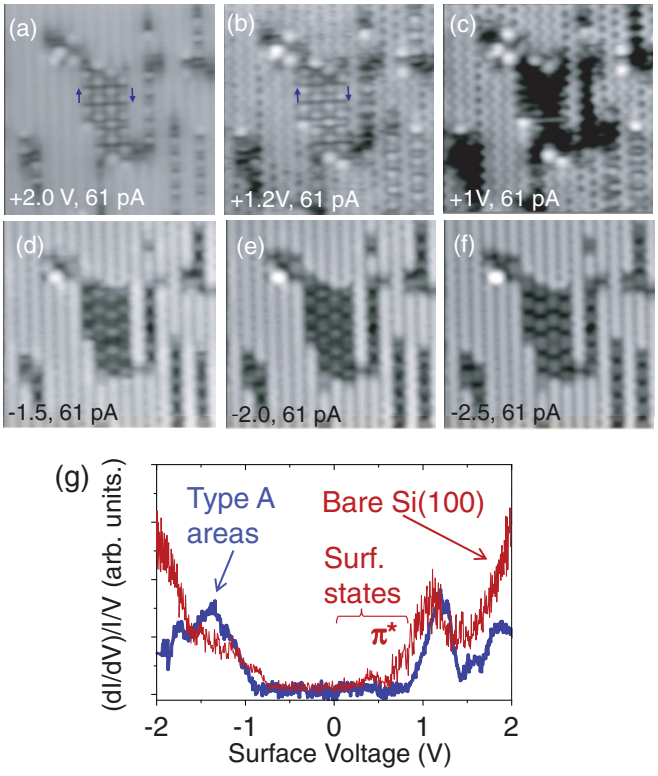

FIG. 4. (Color online) (a) to (c) 146 × 146 Å^2 unoccupied state STM topographies of the structure of type-A acquired at V_s of +2.0, +1.2, and +1.0 V (61 pA), respectively. (d) to (f) 146 × 146 Å^2 occupied state STM topographies of the same area acquired at −1.5, −2.0 and −2.5 V (61 pA), respectively. (g) dI/dV curves acquired on the type-A area and on the bare silicon surface.

bias voltage between experiment and calculations mainly arise from the DFT underestimation of the silicon surface band gap and the relative positioning of the Fermi level between theory and experiment.[24,25] Our DFT calculation estimates a computed surface band gap of the bare Si(100)-2 × 2 around ∼0.2 eV, whereas it is measured experimentally around 1.0 eV.[26–28] Our calculated STM images are thus correlated to experimental topographies without any correcting factor or stretching coefficient. Additionally, the calculated profile along the A-A′ section defined in Fig. 3(b) is displayed in Fig. 3(g). This profile shows that the calculated relative height of the considered Ca adatoms is ∼ 0.61 Å with respect to the Si(100) surface along the back-bond row which is very similar to what is measured in Fig. 2(b).

The second type of observed structure resulting from the deposition of CaF_2 on the Si(100) surface is the feature of type-A as defined in Fig. 1(b). A closer look at these areas at various surface voltages highlights their internal structure. For example, the unoccupied state STM topographies at $V_s = +2$, +1.2, and +1 V (Figs. 4(a) to 4(c)) reveal a quasiperiodic internal structure. The internal elements of the dark areas are arranged along the dimer rows to build structures of various sizes, ranging from one to several dimer rows on the silicon surface. An STM topography is acquired at $V_s =$ +1.0 V to show the $p(2 \times 2)$ buckled reconstruction of the adjacent silicon dimmers.[14] From this, the location of the Si dimers and the internal structure of type-A areas can be derived with precision. In particular, we can observe that the internal structures of type-A are mainly oriented in a head-to-tail (HTT) disposition (see blue arrows in Figs. 4(a) and 4(b)). The occupied state STM topographies for V_s ranging from −1.5 to −2.5 V (Fig. 4(d) to 1(f)) reveal similar internal structural arrangement. In addition to these STM topographies, the electronic properties of these structures can also be characterized. For this purpose, we perform several differential conductance (dI/dV) spectra measurements on both the surface and at various locations inside the dark areas. The ensuing dI-dV curves are averaged for each area, and the final curves are representative of reproducible measurements. The corresponding spectra are shown in Fig. 4(g), and they reveal that the surface gap is slightly enlarged when the dI-dV measurements are performed on the dark structures compared to the bare silicon surface, in particular for V_s ranging between 0 and +1 V. This difference mainly concerns the unoccupied $\pi*$ surface states, which are delocalized along the coupled Si dimers of the silicon dimer rows.[29] This suggests that coupled Si dimers do not exist anymore in the type-A areas, most probably due to the chemical reaction of CaF_2 molecules with the silicon surface.

A detailed comparison of the occupied (Fig. 5(a)) and unoccupied (Fig. 5(b)) state STM topographies of the features of type-A enables us to define a unit cell (red rectangles). The position of the unit cells on the Si surface is determined from the position of the silicon dimers of the bare surface (white circles in Figs. 5(a) and 5(b)). Each unit cell can be repeated, with a particular orientation, to form the observed reconstructed dark area. Consequently, we can observe that the whole area of type-A in Fig. 5 is built either from a shifted arrangement of adjacent and alternatively reversed unit cells (see the white arrows marked A in Figs. 5(a) and 5(b)) or from consecutively translated unit cells along and perpendicular to the Si dimer rows (red arrows marked B in Figs. 5(a) and 5(b)). The first case corresponds to HTT unit cells, while the second case happens when the cells are oriented in the same direction. A closer look at one of these cells reveals its internal density of state distribution (see inserts of Figs. 5(a) and 5(b)).

To understand the structure of the unit cell of the type-A area, we compute the atomic and electronic structure of the unit cell shown in Fig. 6 by taking into account the axial symmetry along the silicon dimer row observed in the structure of type-A (Fig. 5). Several structures of the unit cell containing various products from the CaF_2 molecules are tested. The best agreement between calculated and experimental STM topographies of both occupied and unoccupied states is obtained for the structure shown in Fig. 6. The ensuing unit cell is built from a 3 × 2 silicon slab, in which one silicon dimer is removed and replaced by a single Ca atom. Additionally, two F atoms are chemisorbed on top of the adjacent silicon dimer. With this configuration, we have allowed the distributions of the entire incoming CaF_2 components to be present in the unit cell in a symmetrical way. In Fig. 6, we display the results of the relaxed structure. In Figs. 6(a) and 6(b), we compare the experimental STM topographies for occupied ($V_s = -1.5$ V) and unoccupied ($V_s = +2.0$ V) surface states, respectively, with the calculated images. The calculated profiles along the A-A′ (Fig. 6(a)) and B-B′ (Fig. 6(b)) axes are compared with experimental measurements in Figs. 6(b)

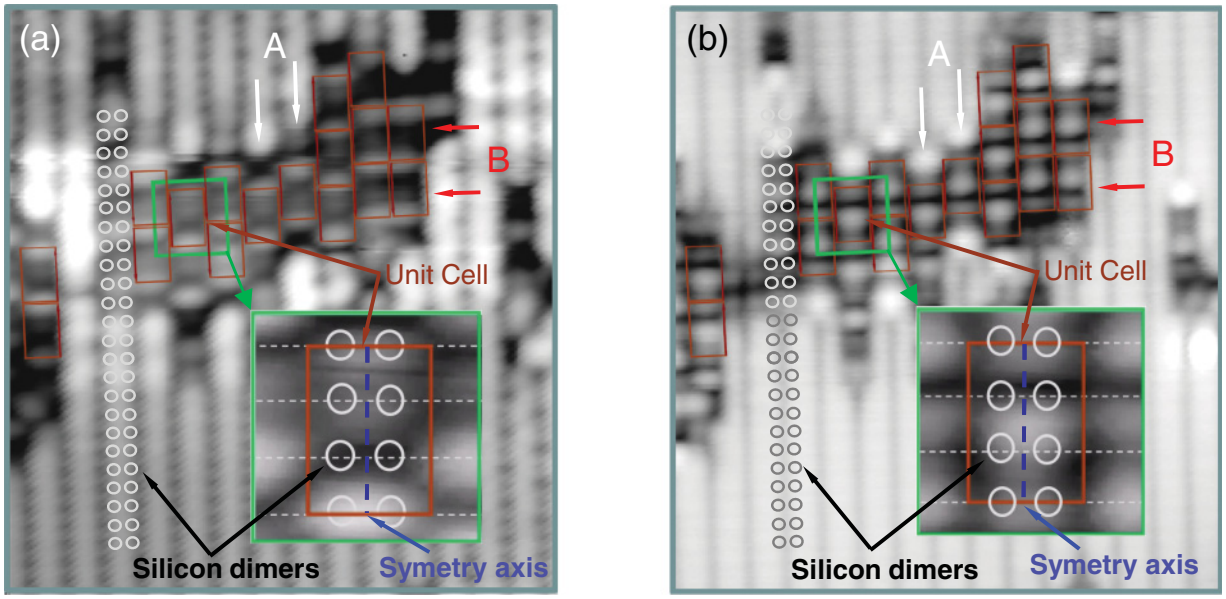

FIG. 5. (Color online) (a) and (b) 115 × 115 Å^2 occupied ($V_s = -1.5$ V, 61 pA) and unoccupied ($V_s = +2.0$ V, 61 pA) STM topographies of a type-A area, respectively. The red rectangles define the unit cells. The white circles indicate the positions of the silicon dimers on the bare surface. The green rectangles define the selected zone of the 15.4 × 15.4 Å inserts.

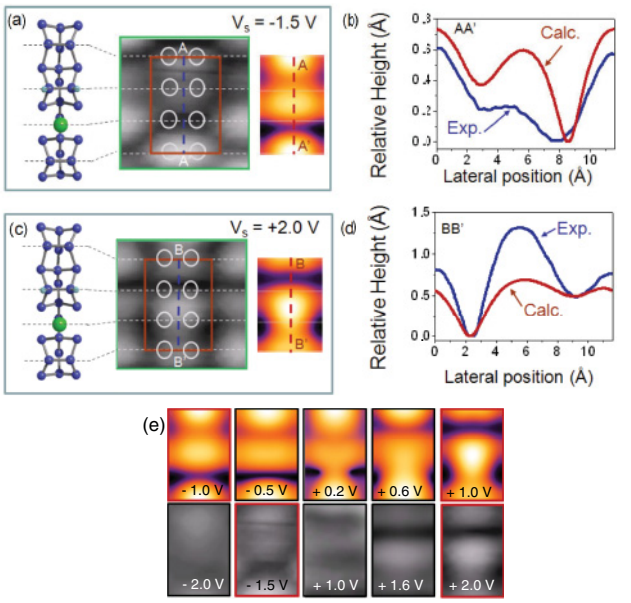

FIG. 6. (Color online) (a) and (c) Comparison of the experimental STM topographies (inserts of Fig. 5) and the calculated STM topographies for the occupied states ($V_s = -1.5$ V, $V_{theo} = -1.0$ V) and unoccupied state ($V_s = +2.0$ V, $V_{theo} = +1.0$ V), respectively. The calculated images were performed with the 3 × 2 Si(100) supercell in which the blue atoms are Si, the green atom is Ca, and the turquoise atoms are F. The doted black/white lines are guidance for the eyes to show the silicon dimer location (light-gray circles). (b) and (d) Comparison between theoretical and experimental averaged profiles along the A-A′ and B-B′ sections taken from (a) and (c), respectively. (e) Comparison between observed and computed STM images for a series of bias voltages $V_s = -2.0$, -1.5, $+1.0$, $+1.6$, and $+2.0$ V, and $V_{theo} = -1.0$, -0.5, $+0.2$, $+0.6$, and $+1.0$ V.

and 6(d). The corresponding experimental profiles arise from numerous measurements (∼20) performed on the various prepared samples. Note that the calculated STM topographies are obtained for bias equal to −1.0 V for the occupied state and +1.0 V for the unoccupied state. Similar to Fig. 3(f), a comparison between calculated STM images and experimental STM topographies of the type-A structure at various voltages is shown in Fig. 6(e). As can be observed in Fig. 6, the calculated topographies of the type-A structure correctly reproduce the experimental ones.

The defined unit cell shown in Fig. 6 allows the two orientations observed in the dark areas of type-A to be described. In particular, the lateral shift between the cells in the HTT configuration of the structure of type-A can be described with more detail, as shown in Fig. 7. When looking at a selected part of Figs. 5(a) and 5(b), we can see (Fig. 7) that the HTT configuration is built via the formation of shifted unit cells, while their relative orientation is reversed on the neighboring dimer rows. As observed in Figs. 7(a) and 7(b) for the occupied and unoccupied density of states STM topographies, the relative shift between two adjacent HTT unit cells is of two silicon dimers. This implies that the formation of the structure of type-A induces the silicon dimers passivated with F atoms to be aligned perpendicular to the dimer rows, as observed in the unoccupied density of state STM topographies of the structure of type-A (Fig. 5(b)).

The proposed structure of the unit cell of type-A areas involves the removal of one silicon dimer. This implies that the silicon surface is partially etched during the adsorption of the CaF_2 molecules, which is consistent with the work of Pasquali *et al.*[11] The removal of the silicon dimers in the presence of F_2 molecules is often explained via the formation of SiF_2 species.[30–32] Although the purpose of this paper is not

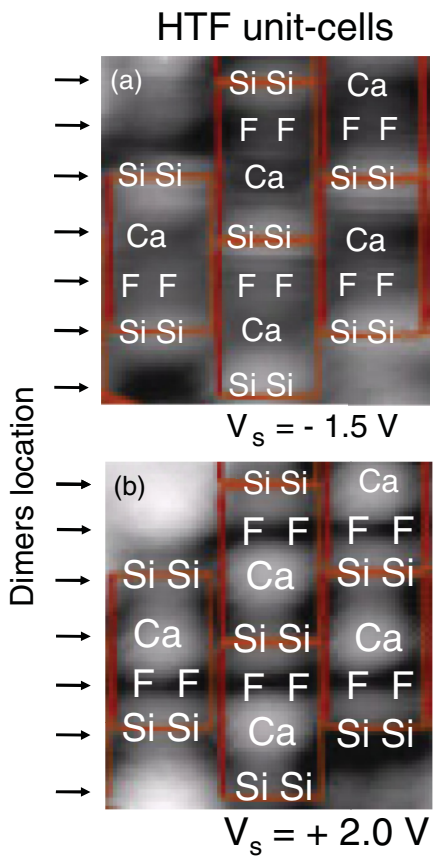

FIG. 7. (Color online) (a) and (b) 23 × 29 Å^2 STM topographies of the occupied ($V_s = -1.5$ V, 61 pA) and unoccupied ($V_s = +2.0$ V, 61 pA) states extracted from Fig. 5. The black arrows allocate the silicon dimers. Si-Si, Ca, and F-F indicate the location of the bare silicon dimers, the Ca adatoms, and the F passivated silicon dimers, respectively, inside the unit cells described by the dark-red rectangle.

focused on the dynamics of the CaF_2 reactivity on the Si(100) surface, we can draw a simple scenario for the fabrication of the observed unit cell if we assume that the Si(100) surface is etched similarly with F_2 or CaF_2 molecules. Therefore, we assume that, preliminary to the silicon etching process with CaF_2, the silicon surface requires a passivation of the silicon dimer with F atoms according to the etching process with F_2 molecules[31] such that:

$$2\,\mathrm{Si} + \mathrm{CaF_2} \rightarrow \mathrm{Ca} + 2\mathrm{SiF}. \quad (1)$$

Thus, to etch a silicon dimer, at least four F atoms are needed to form two desorbing SiF_2 molecules. Consequently, a minimum of two CaF_2 molecules is required for this process, such as:

$$2\mathrm{Si} + 2\mathrm{CaF_2} \rightarrow \mathrm{Ca} + 2\mathrm{SiF} + \mathrm{CaF2} \rightarrow 2\mathrm{Ca} + 2\mathrm{SiF_2}. \quad (2)$$

Following Eq. (2), the two remaining Ca atoms might stay adsorbed on the silicon surface. One of these Ca atoms can be used to fill the missing dimer, while the remaining Ca atoms can either contribute to the fabrication of the observed structures of type-B or desorb from the silicon surface. The process in Eq. (1) can be repeated on the silicon dimers adjacent to the removed silicon dimer to ultimately produce the unit cell with two Si-F bonds, as described previously. However, as observed in our work, the etching process of the Si(100) surface during the deposition of CaF_2 molecules is periodic (one silicon dimer is removed every three dimers of the same dimer row), contrary to what is observed in the presence of fluorine gas, which allows continuous lines of silicon vacancies to be engraved.[31] Thus, the etching of the silicon surface with CaF_2 molecules seems to occur in a different way and restrains the formation of continuous lines of silicon dimer vacancies. The presence of the Ca atom in replacement of the etched dimer in the unit cell might be related to this process. Additionally, we have observed that the relative dispositions of the unit cells in the HTT structure are shifted to produce the formation of adjacent lines of Si-F dimers (see Fig. 7). This configuration is consistent with a passivation process of Si dimers with F atoms prior to the silicon etching. Therefore, the formation of Si-F bonds might also occur at lower coverage rates during CaF_2 exposure.[31] The etching process of the silicon dimer and, therefore, the complete formation of the observed type-A areas require additional CaF_2 molecules, which explains the numerous Ca adatoms forming the observed features of type-B.

IV. CONCLUSION

We have performed the first atomic-scale study of wetting layer formation when the Si(100) surface is exposed to CaF_2 molecules at low coverage (∼0.3 ML). This results in the formation of two types of reacted surface structures. The first one is observed as a complex reconstruction involving a regular arrangement of 3 × 2 unit cells formed with one adsorbed Ca atom and two Si-F bonds. The second structure is made of single Ca adatoms adsorbed on the Si(100) surface. We have shown that both structures result from the dissociation of the CaF_2 molecules when adsorbed on the Si(100). Subsequently, the dissociation of the CaF_2 induces the etching of the silicon surface. The characterization of these observed reacted structures is supported by DFT calculations of their surface geometry and STM topographies. This work emphasize the high-precision analysis offered by the STM methods to investigate the initial-stage formation of ultrathin layers, especially when they are performed at low temperature and combined with DFT calculations. Finally, this work will provide insight for studying the growth of insulating layers on Si(100) at the atomic scale, in particular for the formation of one-dimensional parallel stripes in higher coverage regimes.

ACKNOWLEDGMENTS

This research is part of the project PicoInside (Contract No. FGP-015847). A. S. Foster and H. P. Pinto acknowledge support from the Academy of Finland and generous grants of computing time from the Center for Scientific Computing (CSC) in Espoo, Finland.

*damien.riedel@u-psud.fr

[1] K. Sadakuni, T. Harianto, H. Akinaga, and T. Suemasu, Appl. Phys. Exp. **2**, 063006 (2009).

[2] G. Volpe, G. Molina-Terriza, and R. Quidant, Phys. Rev. Lett. **105**, 216802 (2010).

[3] X. M. Fang, T. Chatterjee, P. J. McCann, W. K. Liu, M. B. Santos, W. Shan, and J. J. Song, Appl. Phys. Lett. **67**, 1891 (1995).

[4] D. Rieger, F. J. Himpsel, U. O. Karlsson, F. R. McFeely, J. F. Morar, and J. A. Yarmoff, Phys. Rev. B **34**, 7295 (1986).

[5] E. Rotenberg, J. D. Denlinger, M. Leskovar, U. Hessinger, and M. A. Olmstead, Phys. Rev. B **50**, 11052 (1994).

[6] M. Vexler, Yu Illarionov, S. Suturin, V. Fedorov, and N. Sokolov, Phys. Solid States **52**, 2357 (2010).

[7] A. A. Velichko, V. A. Ilyushin, D. L. Ostertak, Yu. G. Peisakhovich, and N. I. Filimonova, J. Surf. Invest. **1**, 479 (2007).

[8] S. M. Suturin, N. S. Sokolov, J. Roy, and J. Zegenhagen, Surf. Sci. **605**, 153 (2011).

[9] D. Toton, Ch. D. Lorenz, N. Rompotis, N. Martsinovich, and L. Kantorovich, J. Phys. Condens. Matt. **22**, 074205 (2010).

[10] N. S. Sokolov, and S. M. Suturin, Appl. Surf. Sci. **175–176**, 619 (2001).

[11] L. Pasquali, S. M. Suturin, V. P. Ulin, N. S. Sokolov, G. Selvaggi, A. Giglia, N. Mahne, M. Pedio, and S. Nannarone, Phys. Rev. B **72**, 045448 (2005).

[12] D. Osterak, M. Friedrich, A. Velichko, V. Ilyushin, and D. R. T. Zahn, Thin Solid Films **517**, 4599 (2009).

[13] G. Comtet, G. Dujardin, L. Hellner, M. Lastapis, M. Martin, A. J. Mayne and D. Riedel, Phil. Trans. R. Soc. A **362**, 1217 (2004).

[14] D. Riedel, M. Lastapis, M. G. Martin, and G. Dujardin, Phys. Rev. B **69**, 121301 (2004).

[15] G. Kresse and J. Furthmüller, Phys. Rev. B **54**, 11169 (1996).

[16] G. Kresse and J. Furthmüller, Comput. Mater. Sci. **6**, 15 (1996).

[17] J. P. Perdew, K. Burke, and M. Ernzerhof, Phys. Rev. Lett. **77**, 3865 (1996).

[18] G. Kresse and D. Joubert, Phys. Rev. B **59**, 1758 (1999).

[19] Ashcroft and Mermin, *Solid State Physics* (Sanders College Publishing/Harcourt Brace, Orlanda, Florida, USA, 1980).

[20] J. Tersoff and D. R. Hamann, Phys. Rev. Lett. **50**, 1998 (1983).

[21] K. Palotas and W. A. Hofer, J. Phys. Condens. Matt. **17**, 2705 (2005).

[22] M. Lastapis, M. Martin, D. Riedel, and G. Dujardin, Phys. Rev. B **77**, 125316 (2008).

[23] D. Riedel, M. Cranney, M. Martin, R. Guillory, G. Dujardin, M. Dubois, and P. Sonnet, J. Am. Chem. Soc. **131**, 5414 (2009).

[24] J. Dabrowski and M. Scheffler, Appl. Surf. Sci. **56–58**, 15 (1992).

[25] A. Ramstad, G. Brocks, and P. J. Kelly, Phys. Rev. B **51**, 14504 (1995).

[26] M. Dubois, L. Perdigão, C. Delerue, G. Allan, B. Grandidier, D. Deresmes, and D. Stiévenard, Phys. Rev. B **71**, 165322 (2005).

[27] K. Hata, Y. Shibata, and H. Shigekawa, Phys. Rev. B **64**, 235310 (2001).

[28] L. Perdigão, D. Deresmes, B. Grandidier, M. Dubois, C. Delerue, G. Allan, and D. Stiévenard, Phys. Rev. Lett. **92**, 216101 (2004).

[29] A. Bellec, D. Riedel, G. Dujardin, O. Boudrioua, L. Chaput, L. Stauffer, and P. Sonnet, Phys. Rev. B. **80**, 245434 (2009).

[30] D. L. Flamm, Pure Appl. Chem. **62**, 1709 (1990).

[31] K. S. Nakayama and J. H. Weaver, Phys. Rev. Lett. **83**, 3210 (1999).

[32] D. P. Pullman, A. A. Tsekouras, Y. L. Li, J. J. Yang, M. R. Tate, D. B. Gosalvez, K. B. Laughlin, M. T. Schulberg, and S. T. Ceyer, J. Phys. Chem. B **105**, 486 (2001).